RESEARCH

Ground-state decoherence of lithium atoms by diatomic polar molecules and noble-gas atoms

Kiyoshi Ishikawa[1] · Mayu Yamamoto[1]

Abstract

We report on the ground-state coherence of Li atoms in the vapor of the diatomic polar molecules, LiCl, and in the noble gases, Ne, Ar, and Xe. The decay of spin precession provides insight into the magnetic sublevel decoherence due to spin-rotation and spin-exchange interactions. These interactions are identified by the temperature dependence of sublevel decoherence and evaluated in Ne, Ar, and Xe gases, respectively. The linewidth of coherent population trapping is attributed to a combination of magnetic sublevel and hyperfine-level decoherences. Subtracting the sublevel decoherence, the hyperfine decoherence, indicated by the Carver rate, is obtained in Xe gas. In Ne and Ar gases, the hyperfine decoherence is found to be negligible. When LiCl vapor is added to the noble gases, the polar LiCl molecules broaden both the sublevel and hyperfine resonances of the Li atoms. This broadening is not due to the Carver rate but to spin-rotation interactions with the dilute molecules.

1 Introduction

The lithium (Li) atom is the smallest of alkali metal elements and has a simple energy structure with experimental and theoretical advantage [1, 2]. The saturated vapor becomes optically detectable at temperatures above approximately 220 °C [3–5]. At high translational velocities, atomic quantum characteristics such as pumped population imbalance and coherence are transported ballistically in vacuum and diffusively in the buffer gas. When the atoms reach a cell wall, the atomic states may decay or be transferred to other atoms adsorbed on the surface [6]. One of the most important properties we want to transfer to solids is nuclear spin polarization, which will allow us to polarize most nuclear spins in a solid. Since the radii of Li atoms and ions are small, they should be able to penetrate solid materials while maintaining nuclear spin polarization. Injection of spin-polarized atoms is another means of polarizing solid nuclei.

The above idea was confirmed by polarized cesium atoms [7, 8]. In the experiments, the polarized atoms and spin polarization were injected into hydride, halide crystals, and

silicate glasses [9]. However, the mobility of cesium atoms was too small to spin-polarize the entire material. Heating could increase mobility, but the too-high vapor and optical densities would disturb the spectroscopic experiments. Therefore, the practical application is left to Li atoms, one of the candidates for mobile atoms that transfer spin polarization, because the atomic vapor density, ion mobility in the material [10, 11], and halide vapor density [12] can be optimized in the same temperature range.

At high magnetic fields, the Zeeman interaction of electrons is greater than the hyperfine interaction, and the nuclear spins decoupled from electrons may not be optically polarized. However, in the actual experiments, decoherence processes in low fields, such as the Carver-rate and *S*-damping (spin-rotation) relaxations, facilitate optical polarization of nuclear spins at high fields [8, 13]. Therefore, the collision-induced decoherence of Li atoms could be a crucial process in halide vapor and noble gases. For other alkali atoms, collisional effects have been intensively investigated in noble gases, nitrogen gas, and organic molecules such as methane, ethylene, and paraffin [14]. They are used as buffer gases, quenching gases, and anti-spin-relaxation coatings at room temperature to obtain narrow resonances and long-lived coherence in precision measurements [15, 16]. However, little is known about the spectroscopic parameters of warm Li atoms, which experience many atomic collisions. Up to the present, diffusion coefficients, spin polarization

✉ Kiyoshi Ishikawa
   ishikawa@sci.u-hyogo.ac.jp

[1] Graduate School of Science, University of Hyogo,
   Hyogo 678-1297, Japan

decay [4], hyperfine frequency-shift and coherence [3, 17] have been investigated for Li atoms in noble gases. On the other hand, for all alkali-metal atoms, polar functional groups of the organic molecules as well as polar, smaller molecules can perturb the quantum state of atoms, which has not been studied in vapor cells. Therefore, by studying atomic collisions, it is necessary to find gases with appropriate magnitudes of the Carver and S-damping rates at high temperatures [18].

In this work, the hyperfine coherent population trapping (CPT) and spin free-precession (FP) signals are measured for ground-state ^{7}Li atoms in noble gases. The hyperfine splitting frequency is proportional to the electron density at the Li nucleus [2, 19]. The atomic collisions alter the electron density and thus cause frequency shift and broadening [18, 20]. Polar diatomic molecules, lithium chloride (LiCl) [21], can also perturb the atomic coherence because electric fields reduce the electron density by the mixing of the excited states [22]. Based on the resonance width as a measure of decoherence of the Zeeman and hyperfine levels, we discuss spin-rotation and spin-exchange interactions for sublevel coherence and the Carver rate for hyperfine coherence [13, 23]. We find that the collisions of polar molecules induce additional broadening of both CPT and FP signals. Despite the dilute vapor, the molecules significantly disturb coherent dynamics of atomic states mainly through spin-rotation interactions.

2 Experiment

2.1 Glass Li-vapor cell

The glass vapor cells were manufactured as follows. [4] Pieces of metallic Li (commercial-grade purity) in ceramic crucibles was baked at $400\,°C$ in each optical, spherical cell. The glass bodies of the cells were also baked at the same time. Due to the baking of metal, a thin metallic film was formed on the inner surface of the glass stem. The noble gases (Ne, Ar, and Xe) in stable isotope ratios were, respectively, introduced into the baked cells through the glass stem from a vacuum chamber. Trace impurities in noble gas, such as O_2 and H_2O, could be removed by chemical reaction to the metallic film. The gas pressure was measured at room temperature, and the glass cells were sealed with a gas torch. After sealing, a slight correction was applied to the cell pressure by measuring the pressure change in the chamber. For LiCl vapor, LiCl salt in powder form was baked in a vacuum glass cell at $400\,°C$ before baking Li metal. A stable isotope ratio, ^{6}Li/^{7}Li $= 8/92$, was expected in the Li-vapor cells. The radius of the spherical cells was $R = 25$ mm. The buffer-gas density $N = n/n_0$ is expressed in units of amg, where the number density of buffer gas n, and the number density

of an ideal gas $n_0 = 2.69 \times 10^{19}$ cm^{-3} at a pressure of 1 atm (101.325 kPa) and a temperature of 273.15 K.

2.2 Atomic Li spectroscopy

In the optical experiments, the cell temperature was controlled in an oven between $250\,°C$ (the number density of Li atom is $n_{Li} = 6 \times 10^8$ cm^{-3}) and $360\,°C$ ($n_{Li} = 2 \times 10^{11}$ cm^{-3}) [17, 24]. Although the atomic density in alkali-metal vapors is reported to be generally smaller than the literature value, the density has not been measured by optical method in this work [25]. The laser (optical frequency ν_L) was tuned to the ^{7}Li D_1 and ^{6}Li D_2 lines (wavelength 671 nm), as shown in the middle inset of Fig. 1. These lines coincidentally overlapped within Doppler width (~ 3.5 GHz). Pressure broadening ($0.5 \sim 5$ GHz in the pressure range of this work) was less than the fine splitting (10 GHz) of the excited states $^2P_{1/2}$ and $^2P_{3/2}$ [26, 27]. We measured the CPT signals to study hyperfine coherence and the FP signals to Zeeman sublevel coherence. The details of the experiment have been described [4, 17].

2.2.1 Coherent population trapping

For the CPT signals, two optical beams, which were linearly and orthogonally polarized, propagated along the z axis, as shown in Fig. 1a. The frequency difference between the two beams ν_μ was generated by an
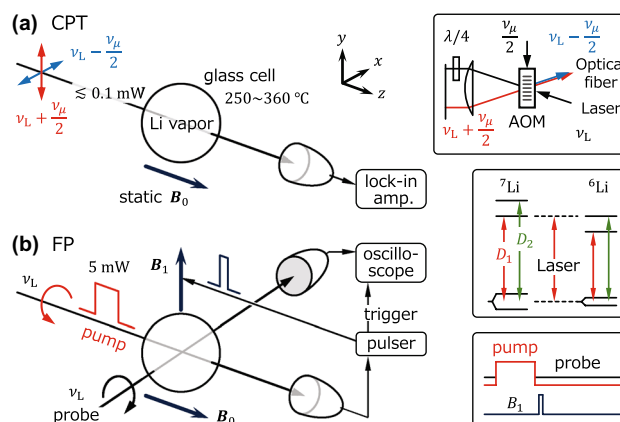

Fig. 1 a Optical alignment for CPT signals of ground state ^{7}Li atoms. Two optical beams were polarized linearly and orthogonally. The static magnetic field $\boldsymbol{B}_0$ was applied along the z axis. The top inset details the setup for scanning the frequency ν_μ by an acousto-optical modulator. The middle inset shows the atomic energy levels and laser tuning. **b** Optical alignment for FP signals. After the optical-pumping pulse along the z axis, the transverse magnetic-field pulse $\boldsymbol{B}_1$ was applied. FP signals were measured with the transmission of the continuous-wave probe light along x axis and averaged over thousands of traces. The pulse sequence is shown in the bottom inset

acousto-optic modulator from the laser light. See the top inset in Fig. 1. The traveling-wave-type modulator allows the frequency ν_μ to be scanned near the splitting frequency ν_{00} of the hyperfine levels $|F = I \pm \frac{1}{2}, m_F = 0\rangle$ of the ground-state ^{7}Li atom (nuclear spin $I = \frac{3}{2}$). At CPT resonance, a part of atoms was pumped into the dark state, a superposition of two hyperfine levels, and light transmittance increased. There were other resonances for $m_F = \pm 1$ on both sides of the center signal for $m_F = 0$. To resolve the center signal at ν_{00} from magnetic-field-sensitive resonances of $m_F = \pm 1$, a static magnetic field B_0 was applied along the optical axis in a magnetic shielding box. The transmitted light power was lock-in detected by modulating the frequency difference ν_μ, resulting in a dispersion-like shape of the signal, as shown in Fig. 2. The modulation frequency was optimized according to the resonance width to improve the signal-to-noise ratio. The relative amplitude of the quadrature-phase signal is an indicator of optimization. If the quadrature signal is too high, the signal shape is distorted, and if it is too low, the signal-to-noise ratio can be improved. Due to the Zeeman shift, the resonances for $m_F = \pm 1$ were out of the frequency scan range. By fitting the simulation curves to the center signals, we obtain the hyperfine splitting frequency and the intrinsic width [5].

Figure 3a shows the center frequency in the gases Ne, Ar, and Xe. The hyperfine splitting frequency in vacuum, $\nu_{00}^{vac} = 803\,504\,105$ Hz, is indicated by dashed horizontal line. The frequency shift depended on the buffer gas, buffer-gas density, and temperature. Even when LiCl vapor coexisted in Ne or Ar gas, the frequency was almost the same within the fitting error as the frequency in each pure noble gas. The linewidth varied with the buffer gas, gas density, temperature, and the presence of LiCl vapor, as shown in Fig. 3b. It should be noted that LiCl vapor
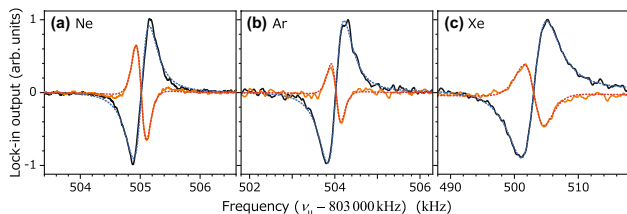

Fig. 3 **a** Hyperfine splitting frequency in the Ne and Ar gases in the presence and absence of LiCl, and in the Xe gas in the absence of LiCl. The error bars show a standard deviation in fitting. The dashed horizontal line is the frequency in vacuum. **b** Full-width at half maximum (FWHM) of CPT resonances. Solid curves show the least-squares fitting of a function, $a + b\exp(cT)$, where T is the temperature in K. **a**, **b** Ne 0.032 amg (3.5 kPa) (•), Ne 0.24 amg (25.8 kPa) (▼), Ne 0.033 amg (3.6 kPa) + LiCl (○), Ar 0.041 amg (4.5 kPa) (▲), Ar 0.039 amg (4.2 kPa) + LiCl (△), Xe 0.023 amg (2.5 kPa) (◆), and Xe 0.049 amg (5.4 kPa) (■)

caused broadening despite its diluteness. The light shift and power broadening have already been subtracted from the measurements.

2.2.2 Spin free precession

For the FP signals, circularly-polarized pump pulses were irradiated along the static magnetic field. See Fig. 1b. The light pulse of a power of 5 mW and a duration of 1 ms was tuned to the ^{7}Li D_1 line. Most of the atoms were pumped to the dark state $|F = 2, m_F = F\rangle$. Other hyperfine levels $|F = 1, m_F\rangle$ were depopulated because the hyperfine splitting was less than the line width of optical absorption. The ^{6}Li atoms were similarly pumped through D_2 line, as shown in the middle inset of Fig. 1. After each optical pulse, a transverse magnetic-field pulse B_1 was applied. The pulse amplitude 24 μT was higher than the static magnetic field B_0, the pulse duration 1.5 μs was smaller than the spin precession period, and the pulse area was $\pi/2$ for ^{7}Li atoms. The pulse B_1 induced the precession of ^{7}Li and ^{6}Li atoms at the respective Larmor frequencies. The precession was probed with weak, continuous, circularly-polarized, and resonant light. The decay of precession due to light absorption was negligible. Since B_0 was kept as uniformly as possible, the decay was assumed to be mainly due to atomic collisions and diffusion. The transmission of probe light was recorded with an oscilloscope and averaged over thousands of traces.

As shown in Fig. 4a, the FP signals were measured with sufficient bandwidth at the precession frequency. With no

Fig. 2 CPT signals of the 0–0 resonance measured at 320 °C in (**a**) Ne 0.032 amg (3.5 kPa) at 0.5 μT, **b** Ar 0.041 amg (4.5 kPa) at 0.5 μT, and **c** Xe 0.023 amg (2.5 kPa) at 5 μT. The gas density is calculated from the pressure at room temperature. The modulation frequency was **a**, **b** 130 Hz, and **c** 1 kHz. The in-phase signals (solid black curves), the quadrature-phase signals (solid orange-color curves) of a lock-in amplifier, and the dotted fitting curves. Note the difference in frequency scan ranges
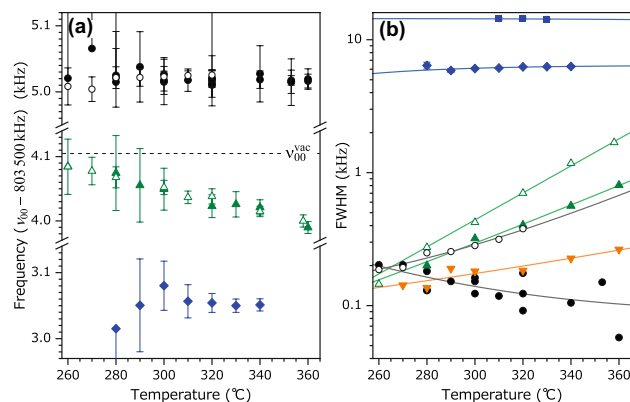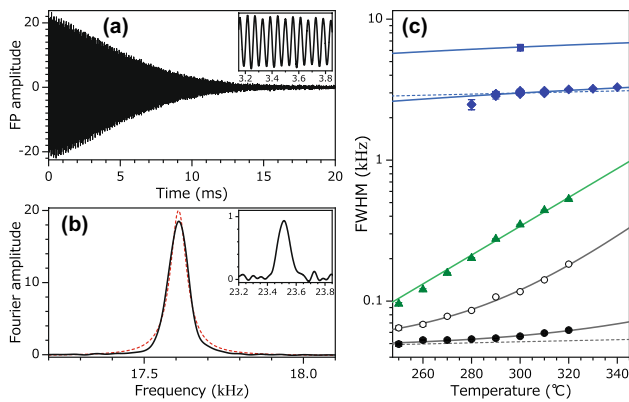
Fig. 4 **a** FP signal in Ne 0.032 amg at 2.5 μT and 320 °C. The inset shows the expanded signal. **b** Fourier transform of the signal in **a** (solid curve) and least-squares fitting of single Lorentzian (dotted curve). The inset shows the spectrum for the ^{6}Li atoms. The vertical axes are in arbitrary units and can be compared with each other. **c** FWHM of the Fourier spectrum in Ne 0.032 amg (•), Ne 0.033 amg + LiCl (○), Ar 0.041 amg (▲), Xe 0.023 amg (◆), and Xe 0.049 amg (■). Solid curves show least-squares fitting of a function, $a + b \exp(cT)$. The dotted curves, $d\sqrt{T}$, are a guide for the eye

phase sensitive detection, the distortion was negligible even at low magnetic fields. The beginning of the signal decayed slightly non-exponentially due to the spin-exchange interaction in the rotating frame [28]. Therefore, the spin-exchange rate between the Li atoms was on the order of the nonlinear Zeeman splitting, which was of 2 Hz at $B_0 = 2.5\ \mu$T, and was sufficiently small compared to other decay rates. Figure 4b shows the Fourier transform of the FP signal. The resonances at slightly-different frequency in the levels $|F = 1, m_F\rangle$ of ^{7}Li atoms were negligibly small because the atoms were depopulated by optical pumping. Therefore, the signal width was determined by fitting a single Lorentz curve. For narrow lines in Ne gas, distortions due to the spin-exchange interaction are seen but are less important for broader lines. The inset shows that the signal amplitude of ^{6}Li atoms was consistent with that of ^{7}Li for the stable isotope ratios. As shown in Fig. 4c, the temperature dependence of the FP width was completely different for noble gas and LiCl vapor. This difference enables us to identify the interaction induced by the collisions.

3 Decay rates in the noble gases

The decay rates of the CPT signal, Γ_{00}, and the FP signal, Γ_Z, are calculated by $\Gamma = \pi \Delta\nu$, where $\Delta\nu$ is a full-width at half maximum of the measured resonance. The rates for the ^{7}Li atoms are expressed, as follows, [13, 29–31]

$$\Gamma_{00} = \Gamma_d + 2\eta_I^2 \Gamma_C + \frac{3}{4}(\Gamma_{sd} + \Gamma_{ex}) + \gamma'_{op}, \tag{1}$$

$$\Gamma_Z = \Gamma_d + \frac{3}{4}(\Gamma_{sd} + \Gamma_{ex}) + \gamma''_{op}, \tag{2}$$

where $\eta_I = \mu_I/(2I\mu_N) = 1.085$, μ_I is the magnetic moment of the ^{7}Li nuclei, and μ_N is the nuclear magneton. The rate Γ_d is due to atomic diffusion in buffer gas and depends on the temperature, buffer-gas density, and dimensions of the laser beam and glass cell. Γ_C is the Carver rate at which the electron spin and the nuclear spin relax in high magnetic fields [23]. Γ_{sd} is the *S*-damping rate due to spin-rotation interaction during the atomic collisions [32]. We neglected *S* damping by the collisions between Li atoms because the Li vapor was dilute at the measurement temperatures. Due to the small spin-orbit splitting in the Li 2*p* orbital, Γ_{sd} mainly comes from the spin-orbit interaction of colliding noble-gas atoms [33]. The rate, $\Gamma_{ex} = \Gamma_{ex}^{ee} + \Gamma_{ex}^{en}$, is from the spin-exchange interaction between the electrons of Li atoms (Γ_{ex}^{ee}) and between the electrons and the buffer-gas nuclei (Γ_{ex}^{en}). Since Γ_{ex}^{ee} was smaller than other decay rates and Larmor frequencies, the Zeeman frequency and width were independent of spin polarization by optical pumping [34, 35]. Because the nuclear spin of noble-gas atoms is unpolarized in our experiment, Γ_{ex}^{en} is simply proportional to the collision rate. It can be significant in the isotopes of Xe gas. The precession state at $\langle F \rangle \perp B_0$ is a superposition of many sublevels. When no beats appear in the FP signal, we can assume that Γ_{sd} and Γ_{ex} are independent of sublevels. Therefore, Γ_Z is independent of sublevels in Eq. (2) [28, 36, 37]. The rates, γ'_{op} and γ''_{op}, come from optical pumping. For the CPT signal, the atoms were pumped to the dark state at a certain level of laser light, i.e., $\gamma'_{op} \neq 0$. Γ_{00} was obtained by extrapolating pump power to $\gamma'_{op} = 0$. For the FP signal, the probe light was weak sufficiently that $\gamma''_{op} \approx 0$. As a result, we obtain from Eqs. (1) and (2),

$$\Gamma_{00} = \Gamma_Z + 2\eta_I^2 \Gamma_C. \tag{3}$$

The temperature dependence of the decay rate is discussed. The lowest spatial mode of atomic diffusion in a buffer gas, sinc($\pi r/R$), decays at the rate $\Gamma_d = (\pi/R)^2 D$, where a diffusion coefficient $D \propto \sqrt{T}/n$. We have assumed that the atoms are unpolarized at the uncoated glass walls of spherical cells [38]. The diffusion coefficient of Li atoms is an order of magnitude larger than that of heavier alkali atoms [39]. Since noble gases have smaller atomic radii than Li atoms, Γ_d in the heavier noble gas is estimated to be about the same as $\Gamma_d = 220\ \text{s}^{-1}$ in He gas at 0.076 amg and 290 °C [4]. As shown in Fig. 3b, the CPT widths in the 0.032 amg (•) and 0.24 amg (▼) Ne gas were of similar magnitude to

each other. This means that the decay at 0.032 amg was mainly due to wall collisions, while at 0.24 amg it was due to atomic collisions [40, 41]. Γ_C, Γ_{sd}, and Γ_{ex}^{en} are expressed as $\Gamma = nv\sigma$, respectively, where σ is the collision cross-section. The relative velocity, $v = \sqrt{8kT/\pi\mu}$, at high temperatures is an order of magnitude greater than those of the heavier alkali atoms at room temperature, where k is the Boltzmann constant and μ is the reduced mass. The S-damping cross-section is sensitive to temperature and Γ_{sd} greatly increases with heating. The rates, Γ_C and Γ_{ex}^{en}, are approximately proportional to $\sqrt{T}$ since the cross-sections are insensitive to temperature [13]. Although all rates are expected to increase with heating, line narrowing was observed in Ne 0.032 amg. One possible reason is inhomogeneous broadening that appears when the temperature distribution is not uniform [20,42]. As shown in Fig. 4c, the FP width depends more strongly than $\sqrt{T}$ in Ne gas (•). As a result, in addition to the inhomogeneous width, Γ_Z consists of Γ_d and Γ_{sd}, and Γ_{00} of Γ_d, Γ_{sd}, and Γ_C in 0.032 amg Ne gas.

Figure 5a shows the decay rates calculated from the CPT and FP widths in Eq. (3), $\Gamma_C = (\Gamma_{00} - \Gamma_Z)/2\eta_I^2$. In Xe gas, the decay rate is significantly large and, as the theoretically predicted Carver rate, shows a weak temperature dependence [13]. Therefore, we obtain $\kappa_C = \Gamma_C/N = 1.8 \times 10^5$ s^{-1}amg^{-1} at 320 °C. In Ne and Ar gases, the calculated rates indicate the residual noise of the decay rates measured in different m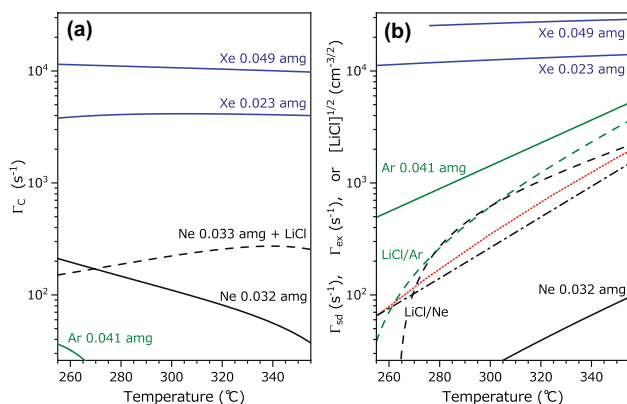ethods, CPT and FP. The noise levels are several orders of magnitude greater than the theoretical Carver rate of 0.4 and 0.1 s^{-1}amg^{-1} in Ne and Ar, respectively [18], and remain too large to discuss an upper bound.

Figure 5b shows the rates, $\frac{4}{3}(\Gamma_Z - \Gamma_d) = \Gamma_{sd} + \Gamma_{ex}^{en}$, calculated from the FP width in Eq. (2). In Ne gas, neglecting Γ_{ex}^{en} in the stable isotopes and subtracting Γ_d (black dotted curve in Fig. 4c), we obtain $\Gamma_{sd}/N = 1.2 \times 10^3$ s^{-1}amg^{-1} at 320 °C. In Ar gas, using $\Gamma_{ex}^{en} \approx 0$ and $\Gamma_d \ll \Gamma_Z$, we obtain $\Gamma_{sd}/N = 5.5 \times 10^4$ s^{-1}amg^{-1} at 320 °C. Because the measured rates show a weak T dependence in Xe gas, using $\Gamma_d \ll \Gamma_Z$ and $\Gamma_{sd} \ll \Gamma_{ex}^{en}$, we obtain $\Gamma_{ex}^{en}/N = 5.8 \times 10^5$ s^{-1}amg^{-1} at 320 °C as the mean in the stable isotopes. Γ_d, Γ_C, Γ_{sd}, and Γ_{ex}^{en} are summarized in Table 1.

The spin-rotation interactions are more pronounced in heavier noble gases, and the signal width also increases with heating [13]. Therefore, Ar gas is one of the suitable buffer gases at room temperature, but not suitable because Γ_{sd} is large in our temperature range. Surprisingly, the interactions appear quite different depending on the temperature range. In Xe gas, Γ_{sd} should be greater than in Ar gas, although it was hidden by the magnitude of Γ_{ex}^{en}. It is necessary to confirm if the rate is insensitive to temperature and remains large even in Xe isotopes with no nuclear dipoles.

4 Decay rates by the LiCl molecules

The LiCl molecule is primarily a dipolar on the potential energy curve of the ground state $X^1\Sigma^+$ [21]. Li$^+$ and Cl$^-$ are, respectively, isoelectronic to He and Ar. Because of the singlet state, the magnetic dipole-dipole interaction between electrons is neglected, i.e., $\Gamma_{ex}^{ee} = 0$. The number density of the molecules increases with heating, but one to two orders of magnitude smaller than the Li density in our temperature range. Therefore, the spin-exchange interaction with the nuclear spin of molecules is insignificant, i.e., $\Gamma_{ex}^{en} = 0$. The change in diffusion coefficient due to the LiCl vapor is also negligible. For Γ_C, the effect of the electric field of the distant polar molecules on the frequency and broadening of atomic signals is negligible because the polarizability of the Li atom, as well as its m_F dependence, are small [19, 22, 43, 44]. As shown in Fig. 3a, no additional shift of frequency ν_{00} due to LiCl vapor was observed in Ne and Ar gas. Figure 5a shows that the Carver rates due to the molecules were similar to or less than the noise levels. Therefore, assuming $\Gamma_C = 0$, we discuss below atomic decoherence due to the spin-rotation interaction.

Figures 3b and 4c show that both CPT and FP signals were additionally broadened by dilute LiCl vapor. Assuming binary collisions of a Li atom, respectively, to a LiCl molecule and a noble-gas atom, we subtract the decay rates measured in the same method, $\Gamma_{00}^{LiCl} - \Gamma_{00} = \Gamma_Z^{LiCl} - \Gamma_Z = (3/4)\Gamma_{sd}^{LiCl}$, in the presence and absence of LiCl vapor in the same noble gas. As shown in Fig. 5b, the subtracted rates indicate a similar

Fig. 5 Γ_C, Γ_{sd}, and Γ_{ex}^{en} calculated from the measured rates, Γ_{00} and Γ_Z. (a) $\Gamma_C = (\Gamma_{00} - \Gamma_Z)/2\eta_I^2$ in Ne (solid black curve), Ne + LiCl (dashed black curve), Ar (solid green curve), and Xe (solid blue curves). (b) Γ_{sd} in Ne (solid black curve), Γ_{sd} in Ar (solid green curve), and Γ_{ex}^{en} in Xe (solid blue curves) are calculated from $\frac{4}{3}(\Gamma_Z - \Gamma_d)$. For LiCl vapor, $\frac{4}{3}(\Gamma_{00}^{LiCl} - \Gamma_{00})$ is calculated in Ne (dashed black curve) and Ar (dashed green curve) and $\frac{4}{3}(\Gamma_Z^{LiCl} - \Gamma_Z)$ in Ne (dotted-dashed black curve). These curves are calculated from the fitting curves in Figs. 3 and 4. The dotted red curve shows $\sqrt{[LiCl]}$, where the number density [LiCl] is extrapolated from those measured above 525 °C [12]

Table 1 The rates $\Gamma_{\rm d}$, $\Gamma_{\rm C}$, $\Gamma_{\rm sd}$, $\Gamma_{\rm ex}^{en}$ for the density of 1 amg and temperature dependence of $\Gamma_{\rm sd}$

$\Gamma_{\rm d}N$ (s^{-1}amg), $\Gamma_{\rm C}/N$, $\Gamma_{\rm sd}/N$, $\Gamma_{\rm ex}^{en}/N$ (s^{-1}amg^{-1}) at 320 °C

	$\Gamma_{\rm d}N$	$\Gamma_{\rm C}/N$	$\Gamma_{\rm sd}/N$	$\Gamma_{\rm ex}^{en}/N$
Ne	5.3(1)	-	$1.2(1)\times10^3$	-
Ar	-	-	$5.5(1)\times10^4$	-
Xe	-	$1.84(2)\times10^5$	-	$5.81(8)\times10^5$

$d(\Gamma_{\rm sd}/N)/dT$ (s^{-1}amg^{-1}°C^{-1}) at 320 °C

Ne	3.3×10^1
Ar	1.3×10^3

$\Gamma_{\rm sd}/N$ (10^3 s^{-1}amg^{-1})

T (°C)	260	280	300	320	340
Ne	0.2	0.4	0.7	1.2	2.0
Ar	13	22	34	55	88

$\Gamma_{\rm sd}$ (10^3 s^{-1}) at the saturated LiCl-vapor density

T (°C)	280	300	320	340
LiCl	0.22	0.50	0.93	1.62

These are calculated from the measured rates, Γ_{00} and $\Gamma_{\rm Z}$, in each pure noble gas and in the presence of LiCl vapor. The mark (–) shows the rate neglected in the calculation. The figure in parentheses shows a standard deviation. $\Gamma_{\rm sd}$ by LiCl vapor is the mean of the three measurements for LiCl in Fig. 5b

temperature dependence within a factor of two. This is additional broadening due to the spin-rotation interaction with the LiCl molecules. Measurable decay rates are obtained even though the LiCl density is much smaller than Li vapor and noble gases. That is, the molecules significantly impact the Li atomic coherence. However, the rate is proportional to $\sqrt{[{\rm LiCl}]}$, where [LiCl] is the LiCl density estimated from the measurements above 525 °C [12]. This indicates that the cross-section is decreased by heating. Further study of the temperature dependence of atomic decoherence by polar molecules is important to elucidate the decoherence mechanism. Using many types of polar molecules, we should consider the magnetic and electric perturbations, Li-LiCl molecular formation, and reactive atom exchange in the warm vapor phase [45, 46].

5 Summary

The hyperfine CPT signals and the spin FP signals of the ground-state ^{7}Li atoms were detected in noble gases. From the signal widths, we measured the Carver rate $\Gamma_{\rm C}$, the S-damping rate $\Gamma_{\rm sd}$, and the spin-exchange rate $\Gamma_{\rm ex}^{en}$ at high temperatures. In Xe gas, the atomic coherence decayed fast due to the significantly large rates, $\Gamma_{\rm C}$ and $\Gamma_{\rm ex}^{en}$. In the Ne and Ar gases, $\Gamma_{\rm sd}$ was measured using $\Gamma_{\rm ex}^{en}=0$ in the stable isotopes. $\Gamma_{\rm C}$ of Li atoms was, similarly to other alkali-metal atoms, too small to be measured in the gases, Ne and Ar. Based on the decay rates measured in pure noble gases, we extracted the collisional

effect of the LiCl molecules on the Zeeman coherence and negligible on the Carver-rate relaxation.

In precision measurements, Ne or Ar gas is mainly used as a buffer gas. He gas is particularly unsuitable for micro-fabricated cells because gas density decreases due to gas permeation through the glass windows. However, in the temperature range where the Li vapor density is high, the atomic decoherence increases due to the spin-rotation interaction with Ar gas. Therefore, Ne gas is the most suitable buffer gas for atomic Li spectroscopy. It is also possible to increase the Carver rate by mixing a small amount of Xe gas because of its relatively small spin-rotation interaction. In combination with the spin–rotation interaction with halide molecules, we expect collision-induced nuclear-spin polarization of Li atoms at high magnetic fields.

Declarations

Conflict of interest The authors declare no conflicts of interest.

References

1. K. Ishikawa, Noble-gas atoms characterized by hyperfine frequency shift of lithium atom. J. Chem. Phys. **156**(14), 144301 (2022)

2. K. Ishikawa, Pseudopotential analysis on hyperfine splitting frequency shift of alkali-metal atoms in noble gases, revisited. J. Chem. Phys. **158**(8), 084306 (2023)

3. J.J. Wright, L.C. Balling, R.H. Lambert, Hyperfine Splittings and Pressure Shifts of Li^6 and Li^7. Phys. Rev. **183**, 180–185 (1969)

4. K. Ishikawa, Spin-polarized lithium diffusion in a glass hot-vapor cell. Appl. Phys. B **122**(8), 224 (2016)

5. K. Ishikawa, M. Inoue, M. Yamamoto, Emission detection of dark resonance in a dilute lithium atomic vapor. J. Opt. Soc. Am. B **39**(9), 2300–2305 (2022)

6. W. Zhen, Wall interactions of spin-polarized atoms. Rev. Mod. Phys. **93**, 035006 (2021)

7. K. Ishikawa, B. Patton, Y.Y. Jau, W. Happer, Spin Transfer from an Optically Pumped Alkali Vapor to a Solid. Phys. Rev. Lett. **98**(18), 183004 (2007)

8. K. Ishikawa, B. Patton, B.A. Olsen, Y.-Y. Jau, W. Happer, Transfer of spin angular momentum from Cs vapor to nearby Cs salts through laser-induced spin currents. Phys. Rev. A **83**(6), 063410 (2011)

9. K. Ishikawa, Hyperpolarized cesium ions doped in a glass material. J. Magn. Reson. **249**, 94–99 (2014)

10. M.J. Weber, Temperature Dependence of Spin-Lattice Relaxation in Alkali Halides. Phys. Rev. **130**, 1–10 (1963)

11. T.G. Stoebe, R.A. Huggins, Measurement of ionic diffusion in lithium fluoride by nuclear magnetic resonance techniques. J. Materials Science **1**(2), 117–126 (1966)

12. D.L. Hildenbrand, W.F. Hall, F. Ju, N.D. Potter, Vapor Pressures and Vapor Thermodynamic Properties of Some Lithium and Magnesium Halides. J. Chem. Phys. **40**(10), 2882–2890 (1964)

13. W. Happer, Y.-Y. Jau, T.G. Walker, *Optically Pumped Atoms* (Wiley-VCH, Weinheim, 2010)

14. C.W. Beer, R.A. Bernheim, Hyperfine pressure shift of ^{133}Cs atoms in noble and molecular buffer gases. Phys. Rev. A **13**, 1052–1057 (1976)

15. D. Budker, M. Romalis, Optical magnetometry. Nat. Phys. **3**(4), 227–234 (2007)

16. O. Katz, O. Peleg, O. Firstenberg, Coherent Coupling of Alkali Atoms by Random Collisions. Phys. Rev. Lett. **115**, 113003 (2015)

17. K. Ishikawa, Pressure effect on hyperfine CPT resonance of ground-state Li atoms in glass hot-vapor cell. Appl. Phys. B **125**(6), 112 (2019)

18. J.C. Camparo, Semiempirical theory of Carver rates in alkali/noble-gas systems. J. Chem. Phys. **126**(24), 244310 (2007)

19. B.H. McGuyer, Hyperfine-frequency shifts of alkali-metal atoms during long-range collisions. Phys. Rev. A **87**, 054702 (2013)

20. P.J. Oreto, Y.-Y. Jau, A.B. Post, N.N. Kuzma, W. Happer, Buffer-gas-induced shift and broadening of hyperfine resonances in alkali-metal vapors. Phys. Rev. A **69**, 042716 (2004)

21. Y. Kurosaki, K. Yokoyama, Ab initio MRSDCI study on the low-lying electronic states of the lithium chloride molecule (LiCl). J. Chem. Phys. **137**(6), 064305 (2012)

22. P.C. Gibbons, N.F. Ramsey, Electric Field Dependence of the Atomic-Hydrogen Hyperfine Separation. Phys. Rev. A **5**, 73–78 (1972)

23. M. Arditi, T.R. Carver, Pressure, Light, and Temperature Shifts in Optical Detection of 0–0 Hyperfine Resonance of Alkali Metals. Phys. Rev. **124**(3), 800–809 (1961)

24. A.N. Nesmeyanov, *Vapor pressure of the chemical elements* (North-Holland, Amsterdam, 1963)

25. Z. Wu, M. Kitano, W. Happer, M. Hou, J. Daniels, Optical determination of alkali metal vapor number density using Faraday rotation. Appl. Opt. **25**(23), 4483–4492 (1986)

26. A. Gallagher, Noble-gas broadening of the Li resonance line. Phys. Rev. A **12**, 133–138 (1975)

27. C.J. Sansonetti, C.E. Simien, J.D. Gillaspy, J.N. Tan, S.M. Brewer, R.C. Brown, S. Wu, J.V. Porto, Absolute Transition Frequencies and Quantum Interference in a Frequency Comb Based Measurement of the ^{6,7}LiD Lines. Phys. Rev. Lett. **107**, 023001 (2011)

28. S. Li, P. Vachaspati, D. Sheng, N. Dural, M.V. Romalis, Optical rotation in excess of 100 rad generated by Rb vapor in a multipass cell. Phys. Rev. A **84**, 061403 (2011)

29. J. Vanier, C. Audoin, *The Quantum Physics of Atomic Frequency Standards* (Adam Hilger, Bristol, 1989)

30. S. Appelt, A. Ben-Amar Baranga, C. J. Erickson, M.V. Romalis, A.R. Young, W. Happer, Theory of spin-exchange optical pumping of He^3 and Xe^{129}. *Phys. Rev. A*, 58:1412–1439 (1998)

31. Yuan-Yu Jau, *New studies of optical pumping, spin resonances, and spin exchange in mixtures of inert gases and alkali-metal vapors*. PhD thesis, Princeton University (2005)

32. R.A. Bernheim, Spin Relaxation in Optical Pumping. J. Chem. Phys. **36**(1), 135–140 (1962)

33. T.G. Walker, W. Happer, Spin-exchange optical pumping of noble-gas nuclei. Rev. Mod. Phys. **69**, 629–642 (1997)

34. W. Happer, H. Tang, Spin-Exchange Shift and Narrowing of Magnetic Resonance Lines in Optically Pumped Alkali Vapors. Phys. Rev. Lett. **31**, 273–276 (1973)

35. S. Appelt, A. Ben-Amar Baranga, A.R. Young, W. Happer, Light narrowing of rubidium magnetic-resonance lines in high-pressure optical-pumping cells. *Phys. Rev. A*, 59:2078–2084 (1999)

36. K. Ishikawa, T. Yabuzaki, Diffusion coefficient and sublevel coherence of Rb atoms in N$_2$ buffer gas. Phys. Rev. A **62**, 065401 (2000)

37. K. Ishikawa, T. Kojima, T. Hasegawa, Y. Takagi, Spin dynamics of dense alkali-metal atoms. Phys. Rev. A **65**, 032511 (2002)

38. F.A. Franz, E. Lüscher, Spin Relaxation of Optically Pumped Cesium. Phys. Rev. **135**, A582–A588 (1964)

39. A. Pouliot, G. Carlse, H.C. Beica, T. Vacheresse, A. Kumarakrishnan, U. Shim, S.B. Cahn, A. Turlapov, T. Sleator, Accurate determination of an alkali-vapor-inert-gas diffusion coefficient using coherent transient emission from a density grating. Phys. Rev. A **103**, 023112 (2021)

40. Jacques Vanier, Jean-F. Simard, Jean-S, Boulanger. Relaxation and frequency shifts in the ground state of Rb^{85}. *Phys. Rev. A*, 9:1031–1040 (1974)

41. T. Lindvall, M. Merimaa, I. Tittonen, E. Ikonen, *All-Optical Atomic Clock Based on Dark States of* ^{85}Rb, pages 183–190. World Scientific, (2002)

42. K. Ishikawa, Noble-gas performance for lithium atomic spectroscopy in glass vapor cells. Appl. Phys. B **128**(1), 7 (2022)

43. Taesul Lee, T.P. Das, R.M. Sternheimer, Perturbation theory for the Stark effect in the hyperfine structure of alkali-metal atoms. *Phys. Rev. A*, 11:1784–1786 (1975)

44. A. Godone, D. Calonico, F. Levi, S. Micalizio, C. Calosso, Stark-shift measurement of the $^2S_{1/2}$, $F = 3 \rightarrow F = 4$ hyperfine transition of ^{133}Cs. Phys. Rev. A **71**, 063401 (2005)

45. Ronald R. Herm. Reactive Scattering of Alkali Atoms and Alkali Halides at Thermal Energies. In P. Davidovits and D.L. McFadden, editors, *Alkali Halide Vapors*, pages 189–253. Academic Press (1979)

46. R.V. Krems, A. Dalgarno, Quantum-mechanical theory of atom-molecule and molecular collisions in a magnetic field: Spin depolarization. J. Chem. Phys. **120**(5), 2296–2307 (2004)